Supporting Information for "Record-Breaking Precipitation in Indonesia's Capital Jakarta in January 2020 Linked to the Northerly Surge, Equatorial Waves, and MJO"

Sandro W. Lubis[1] *, Samson Hagos [1], Eddy Hermawan [2], Muhamad R. Respati [3], Ainur Ridho [4], Risyanto [2], Fadhlil R. Muhammad [5], Jaka A. I. Paski [6], Siswanto [6], Dian Nur Ratri [6,7], Sonny Setiawan [8], Donaldi S. Permana [6]

[1]Pacific Northwest National Laboratory, Richland, Washington, USA

[2]National Research and Innovation Agency (BRIN), Indonesia

[3]School of Earth, Atmosphere and Environment, Monash University, Australia

[4]Search Engine for Risk and Actions on Resilience, Indonesia

[5]School of Earth Sciences, University of Melbourne, Australia

[6]Indonesia Agency for Meteorology Climatology and Geophysics, Indonesia

[7]Wageningen University and Research, Netherlands

[8]Department of Geophysics and Meteorology, IPB University, Indonesia

*902 Battelle Blvd, Richland, WA 99354, USA

Contents of this file

1. Text S1 to Sx
2. Figures S1 to Sx
3. Tables S1 to Sx

Text S1. Relative moisture source contributions

For calculating the moisture sources proportion, we divided the moisture source area into four land regions and four ocean regions; the demarcation map can be seen in Fig. S1. The method for calculating the moisture source's proportion to the target area is based on a Lagrangian diagnostic, similar to Nie and Sun (2022). We evaluate the moisture changes using the inverse of backward trajectories from an ensemble member trajectory with an initial height of 500 m to 2000 m around Jakarta. A moisture source attribution is identified by the location of increasing change in the specific humidity of a particle or evaporation event during a transport time interval. Decreasing change in the specific humidity during a transport time interval is calculated as a precipitation event. The final moisture source proportion from the source area to the target location is weighted by considering a series of precipitation and evaporation events en route.

Text S2. Local phase diagram

In this method, wave-filtered OLR anomalies are first averaged over 10°S-5°S, corresponding to the location of the observation. The annual cycle is removed before the filtering by subtracting the first three harmonics. The linear trend is then removed from the anomalous fields, and a split-cosine-bell tapering is applied to about 10% of both ends of the time series to minimize the spectral leakage. The latitudinal averaged OLR anomaly and its time derivative are then standardized by dividing them by their respective global standard deviations. These values are then plotted in eight phases, according to their amplitude, the phases 4-6 indicate enhanced regional convection by the equatorial

wave, whereas warm colors (phases 8, 1-2) correspond to suppressed regional convection. This method has been widely used to study the regional influence of equatorial waves on precipitation in many other locations (e.g., van der Linden, Fink, Pinto, Phan-Van, and Kiladis (2016); Schlueter, Fink, Knippertz, and Vogel (2019); Lubis and Respati (2021); Latos et al. (2021)).

Text S3. Water vapor transport and moisture flux convergence

The IVT and VIMFC are calculated from total fields and then filtered with respect to the different frequency-wavenumber (see Table S1). The IVT is calculated using ERA5 zonal and meridional winds and specific humidity as follow:

$$\mathrm{IVT} = \left[\left(\frac{1}{g} \int qu \ \mathrm{d}p \right)^2 + \left(\frac{1}{g} \int qv \ \mathrm{d}p \right)^2 \right]^{1/2} \tag{1}$$

where q is specific humidity, u is zonal wind, and v is meridional wind. The VIMFC is calculated from the moisture budget equation:

$$-\frac{1}{g} \int \left(\frac{\partial q}{\partial t} \right) \ \mathrm{d}p \underbrace{-\frac{1}{g} \int \left(\vec{\nabla} \cdot q\vec{V} \right) \ \mathrm{d}p}_{\mathrm{VIMFC}} - \frac{1}{g} \int \left(\frac{\partial \left(q\omega \right)}{\partial p} \right) \ \mathrm{d}p = P - E \tag{2}$$

where $\vec{V}$ is horizontal wind, ω is vertical velocity, P is precipitation, and E is evaporation. VIMFC is a good measure to equatorial wave and MJO modulation on rainfall as it is directly related to the net precipitation (Lubis & Respati, 2021).

References

Latos, B., Lefort, T., Flatau, M. K., Flatau, P. J., Permana, D. S., Baranowski, D. B., ... others (2021). Equatorial waves triggering extreme rainfall and floods in southwest sulawesi, indonesia. *Monthly Weather Review*, *149*(5), 1381–1401.

Lubis, S. W., & Respati, M. R. (2021). Impacts of convectively coupled equatorial waves on rainfall extremes in java, indonesia. *International Journal of Climatology*, *41*(4), 2418–2440.

Nie, Y., & Sun, J. (2022). Moisture sources and transport for extreme precipitation over henan in july 2021. *Geophysical Research Letters*, *49*(4), e2021GL097446. doi: https://doi.org/10.1029/2021GL097446

Schlueter, A., Fink, A. H., Knippertz, P., & Vogel, P. (2019). A systematic comparison of tropical waves over northern africa. part i: Influence on rainfall. *Journal of Climate*, *32*(5), 1501 - 1523. doi: 10.1175/JCLI-D-18-0173.1

van der Linden, R., Fink, A. H., Pinto, J. G., Phan-Van, T., & Kiladis, G. N. (2016). Modulation of daily rainfall in southern vietnam by the maddenjulian oscillation and convectively coupled equatorial waves. *Journal of Climate*, *29*(16), 5801 - 5820. doi: 10.1175/JCLI-D-15-0911.1

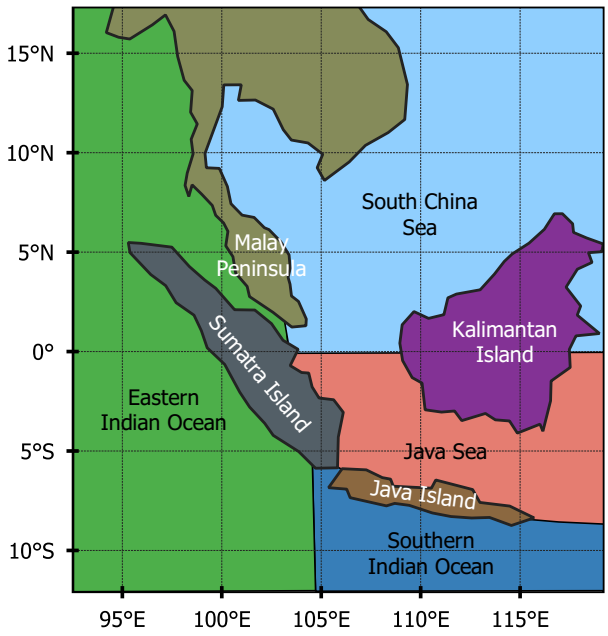

Figure S1. The division of 8 regions, including four land regions and four ocean regions, for the moisture source contribution analysis. The land regions include Sumatra Island, Java Island, Kalimantan Island and the Malay Peninsula. The ocean regions include the the South China Sea, the Java Sea, the eastern Indian Ocean and the southern Indian Ocean.

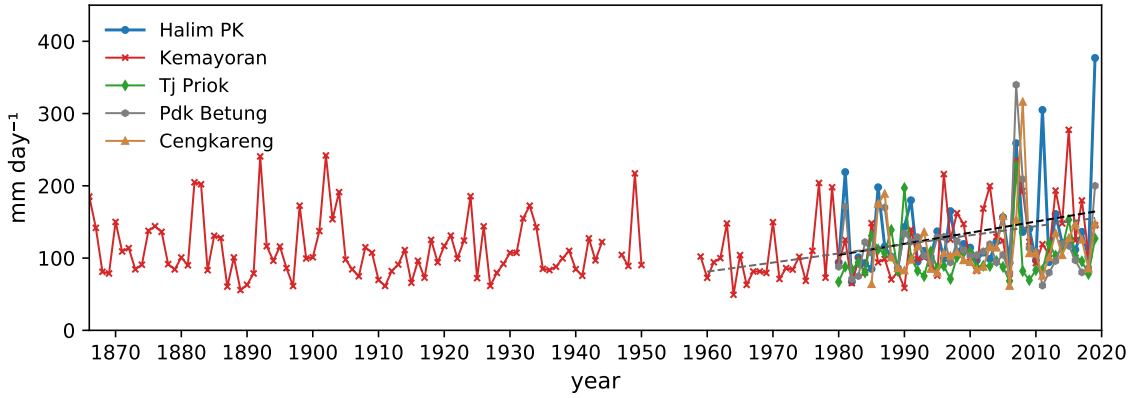

Figure S2. Time series of annual maximum daily precipitation (RX1 day) from 5 rain gauge stations from 1960-1900 (note: only data from Kemayoran station is available back to 1866). The precipitation trend corresponding to the year 1960-2020 (1980-2020) at Kemayoran (Halim) is 12.23 (15.41) mm/decade.

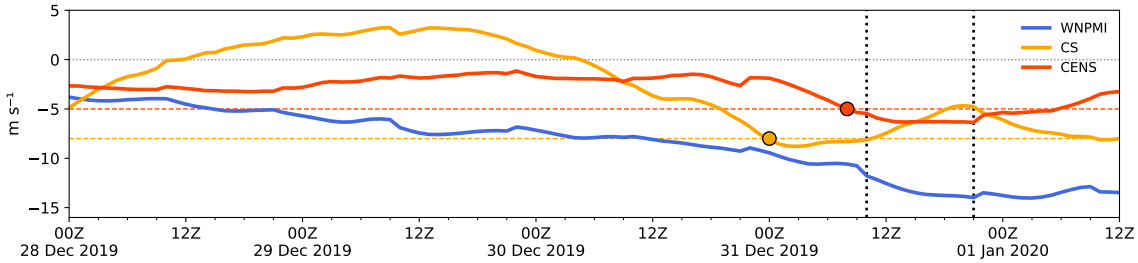

Figure S3. Hourly evolution of cold surge (CS), cross-equatorial northerly surge (CENS), and western North Pacific monsoon index (WNPMI) indices from 0000 UTC 28 December 2019 to 1200 UTC 1 January 2020. The red (orange) circle indicates the period when CENS (CS) is active (i.e., exceeding 5 m s^{-1} for CENS (red line) and 8 m s^{-1} for CS (orange line)). The two vertical lines indicate the first and second peaks of the precipitation (i.e., at 10Z and 22Z, respectively). The WNPMI is defined as the difference of 850-hPa zonal wind between a southern region (5°-15°N, 100°-130°E) and a northern region (20°-30°N, 110°-140°E).

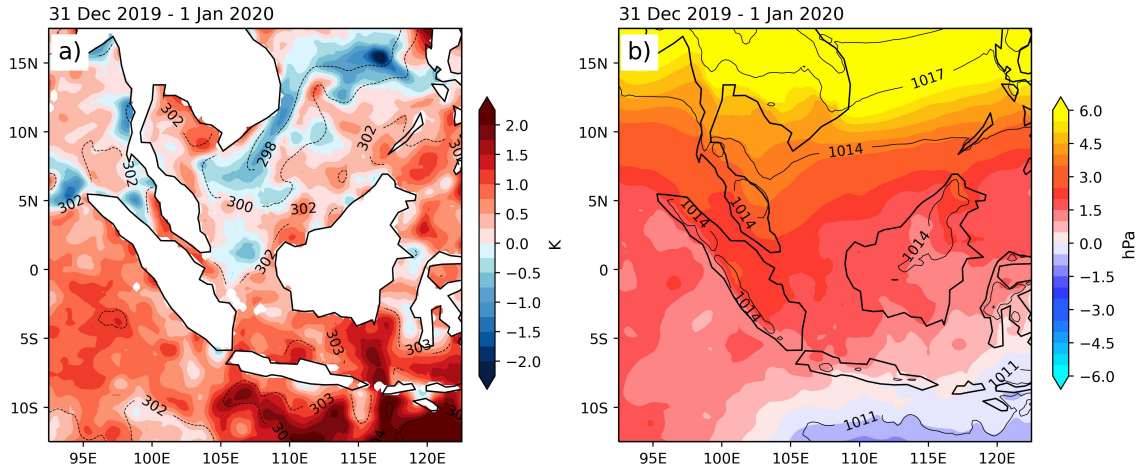

Figure S4. (a) Sea surface temperature (SST) and (b) mean sea-level pressure (MSLP) anomalies averaged from 31 December 2019 to 1 January 2020. Superimposed black contours are the corresponding total field.

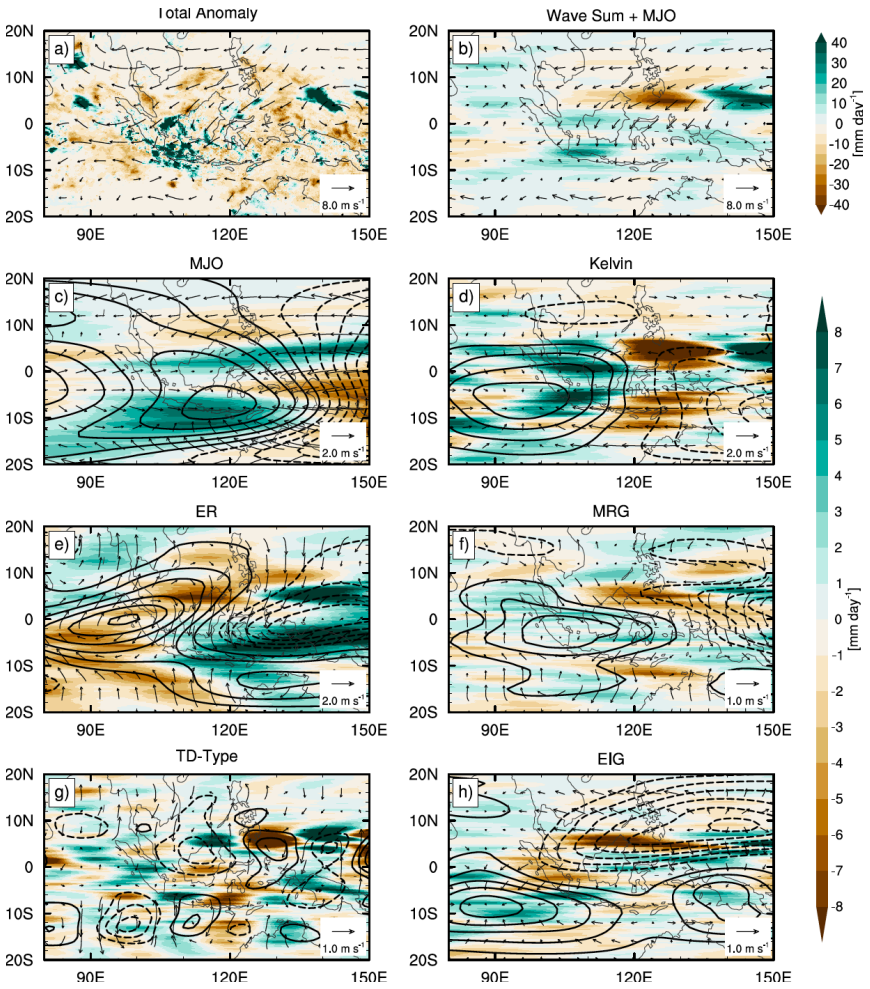

Figure S5. Contribution of different types of CCEWs and MJO on the total daily precipitation anomalies (color shading) during the extreme precipitation event on 31 December 2019. (a) Total anomalies and their corresponding wind vector anomalies, (b) CCEWs- and MJO-filtered anomalies and their corresponding wind vector anomalies, (c) MJO-filtered anomalies and their corresponding divergent wind vectors, (d) Kelvin wave-filtered anomalies and their corresponding divergent wind vectors, (e) ER wave-anomalies and their corresponding rotational wind vectors, (f) MRG wave-filtered anomalies and their corresponding rotational wind vectors, (g) TD-type wave-filtered anomalies and their corresponding rotational wind vectors, and (h) EIG wave filtered anomalies and their corresponding divergent wind vectors. Solid (dashed) contours lines in (e, f, g) indicate positive (negative) values of the stream function anomalies at interval of 5.0 $\times$ 10^6 m^2s^{-1}. Solid (dashed) contours lines in (c, d, h) indicate positive (negative) values of the velocity potential anomalies at an interval of 3.0 $\times$ 10^6 m^2s^{-1}.

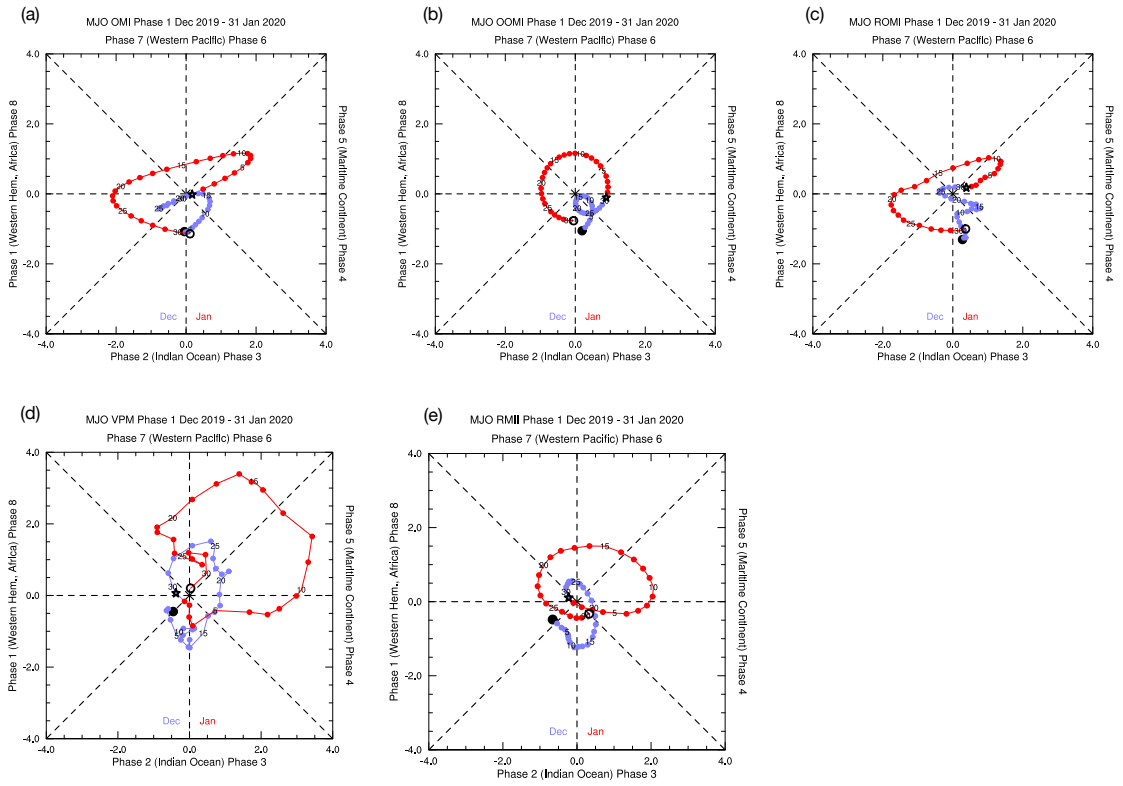

Figure S6. Global MJO indices from 1 December 2019 to 31 January 2020. (a) OLR MJO index (OMI), (b) original OLR MJO Index (OOMI), (c) real-time OLR MJO index (ROMI), (d) velocity potential MJO multivariate index (VPM), and (e) realtime multivariate index for tropical intraseasonal oscillations (RMII). The star indicates the period of the extreme precipitation event on 31 December 2019.

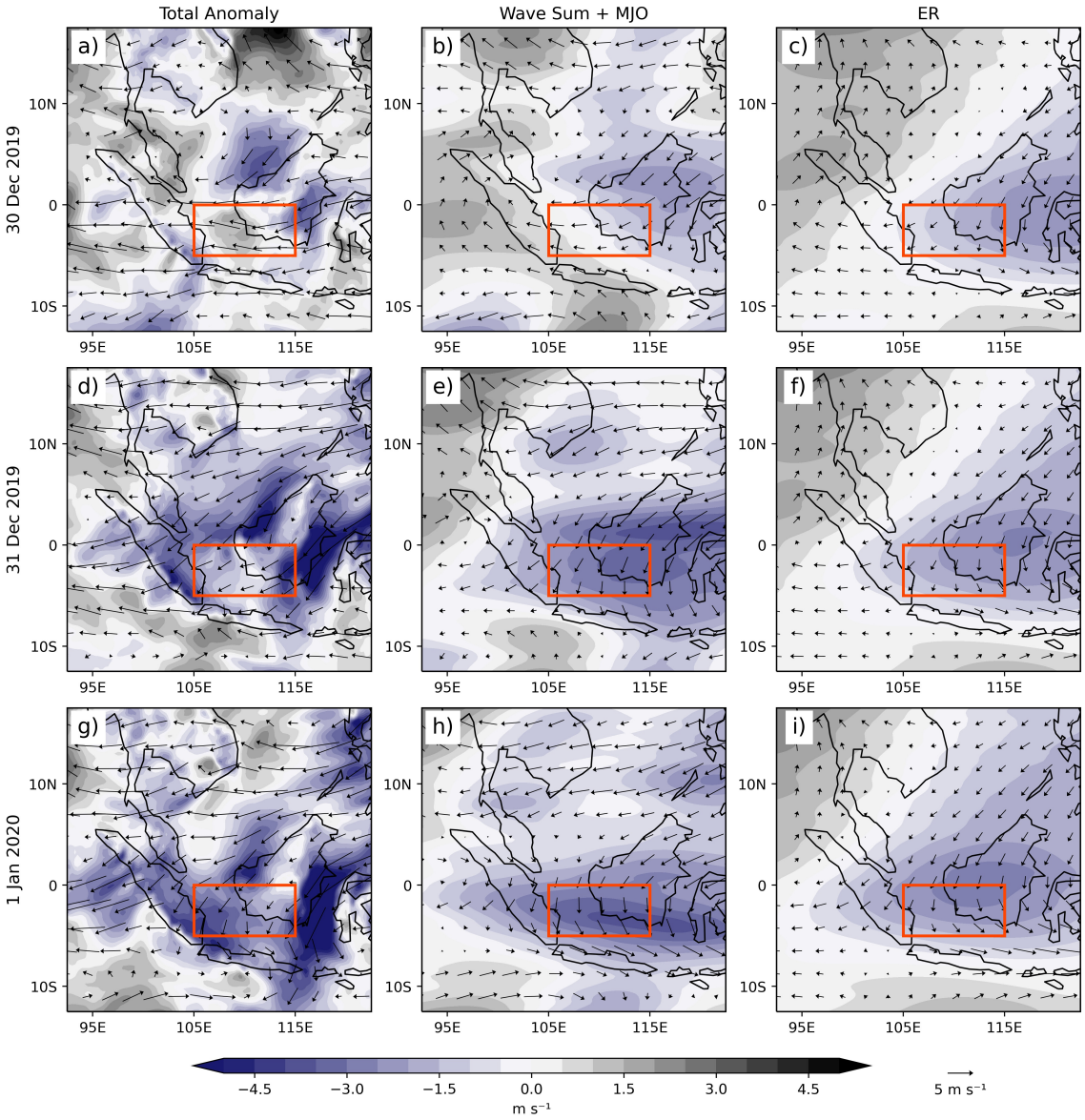

Figure S7. Time evolution of daily mean meridional wind (color shading) and horizontal wind vector anomalies at 925 hPa from 30 December 2019 to 1 January 2020. (a, d, g) Total anomalies, (b, e, h) sum of CCEWs- and MJO-filtered anomalies and (c, f, i) ER wave-filtered anomalies. The red rectangular box indicates the area where CENS is defined.

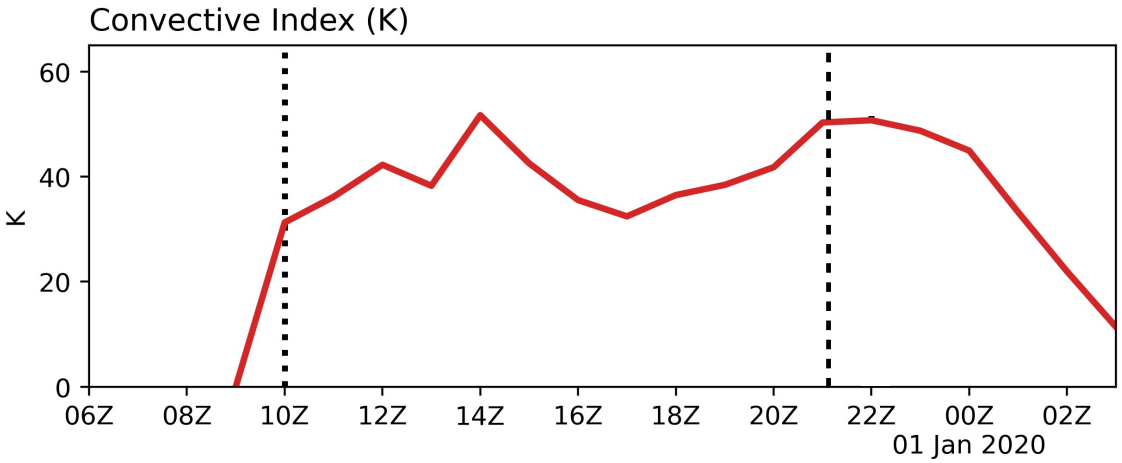

Figure S8. Hourly evolution of convective index (CI) defined by taking temperature below a threshold value of equivalent black body temperature. The threshold value used is 253 K as a measure of convective clouds. CI is averaged over the flood region (regional box in Fig.1a). The two vertical lines indicate the first and second peaks of the observed precipitation (i.e., at 10Z and 21Z, respectively).

Table S1. The period, wavenumber, and equivalent depth used for isolating CCEWs.

Wave Mode	Periods (days)	Wavenumber	Depth (m)
Kelvin	2.5 - 17	1 - 14	8 - 90
Equatorial Rossby (ER)	9 - 72	1 - 10	8 - 90
Mixed Rossby-gravity (MRG)	3 - 10	1 - 10	8 - 90
Eastward Inertio Gravity (EIG) n=0	1 - 5	1 - 14	12 - 50
Tropical-depression (TD)-type	2.5 - 5	6 - 20	-